15th International Conference on
AEROSPACE SCIENCES & AVIATION TECHNOLOGY,
ASAT - 15 – May 28 - 30, 2013, Email: asat@mtc.edu.eg ,
Military Technical College, Kobry Elkobbah, Cairo, Egypt,
Tel: +(202) 24025292 –24036138, Fax: +(202) 22621908

Flight Dynamics, Stability and Control of a Flexible Airplane

A. Khalil*, M. M. ElNomrossy†, G. M. Elbayoumi‡ and M. S. Bayoumi§

Abstract: The paper presents a method for obtaining the flight dynamics, stability and control characteristics of flexible airplanes. Computational fluid dynamics techniques are used for the aerodynamics, while finite element techniques are used to evaluate structure deformations. The coupling between aerodynamics and structure is done by using multi-field Fluid Structure Interaction. Results are generated for an example airplane that has high aspect-ratio wing and fin fuselage. The results indicate that aerodynamic derivatives, static and dynamic stability are changed with dynamic pressure. Results also indicate that the controller design (gain scheduling) for an example automatic flight control system, pitch-attitude hold, has some changes. Furthermore, flight simulation based on fourth-order Runge-Kutta numerical integration indicates small changes on airplane's trajectory during a pull-up maneuver.

Keywords: Flight dynamics, flexible airplane, aerodynamic derivatives, ANSYS multi-field MFX, fluid structure interaction FSI.

Introduction

Airplanes fly at different altitudes and Mach numbers leading to changes in aerodynamic loads applied on their structures which lead to structure deformation. These deformations, in turn, change the airplane shape; hence, the aerodynamic and control characteristics are changed. Ref. [1] gives mathematical formulation for coupling aerodynamics to structure and showing its effect on a highly flexible flying wing. Ref. [2] extends the work of Ref. [1] for a highly flexible airplane. Ref. [3] does this coupling by using classical aerodynamic and structural theories. In this paper the assumption is made that the changes in aerodynamic loading take place so slowly that the structure is, at all times, in static equilibrium. This is equivalent to assuming that structure's natural frequencies of vibration are much higher than the frequencies of rigid-body motion. Thus a change in load produces a proportional change in the shape of the airplane (quasi-static deflections), which in turn influences the load; Ref. [10] .The paper is organized in 6 main sections, including this one. Section 2 represents the governing equations for booth aerodynamics and structure. In section 3, the governing equations for stability and control are written. Section 4 represents a method for obtaining the aerodynamic derivatives of a rigid airplane using CFD techniques. In section 5, a flexible

* Teaching Assistant, Aerospace Engineering Department, Cairo University, Giza, Egypt, ahmed.khalil.ali@eng.cu.edu.eg .
† Professor, Production, Energy and Automatic Control Department, French University in Egypt, Cairo, Egypt, elnomrossy@gmail.com .
‡ Professor, Aerospace Engineering Department, Cairo University, Giza, Egypt, gelbayoumi@yahoo.com .
§ Associate Professor, Aerospace Engineering Department, Cairo University, Giza, Egypt, msb0100@yahoo.com .

airplane is presented and its aerodynamic derivatives are evaluated as function of the dynamic pressure. Section 6 shows the effect of flexibility on static and dynamic stability, automatic flight control system design, and on motion simulation for the flexible airplane presented in section 5.

Aerodynamics and Structure Governing Equations

In this section, the governing equations for booth aerodynamics and structure are written.

Aerodynamics Governing Equations

In this section, the instantaneous equations of mass and momentum are presented. For turbulent flows, the instantaneous equations are averaged leading to additional terms. These equations can be written in a stationary frame leading to Eqns. 1 and 2 for mass and momentum, respectively. The equations are then discretized with a finite element based technique and solved using ANSYS CFX.

$$\frac{\partial \rho}{\partial t} + \nabla.(\rho V) = 0 \tag{1}$$

$$\frac{\partial (\rho V)}{\partial t} + \nabla.(\rho V \otimes V) = -\nabla P + \nabla.\tau + S_M \tag{2}$$

$$\tau = \mu(\nabla V + (\nabla V)^T - \frac{2}{3}\delta \nabla.V) \tag{3}$$

where ρ is density, t is time, V is total velocity vector, P is pressure, μ is dynamic viscosity, τ is stress tensor, and δ is strain rate.

Structure Governing Equations

Static analysis is used to determine displacements, stresses, strains and forces under static loading conditions that do not induce significant inertia and damping effects, such as those caused by time-varying loads. A static analysis can, however, include steady inertia loads (such as gravity and rotational velocity), and time-varying loads that can be approximated as static equivalent loads (such as static equivalent wind). Steady loading and response conditions are assumed; that is, the loads and the structure's response are assumed to vary slowly with respect to time. A finite element solver, ANSYS Static Structural, is used to solve the governing equations. The elements used for finite element modeler are four elements as follows:

10-Node Quadratic Tetrahedron, SOLID187

This element is used to model the spars and rips of wing, tail and fuselage.

4-Node Linear Quadrilateral Shell, SHELL181

This element is used to model the skin of wing, tail and fuselage.

Quadratic Triangular Target, TARGE170

This element is used in conjunction with CONTA173 to contact skin to the spars and ribs.

Linear Triangular Contact, CONTA173

CONTA173 is used to represent contact and sliding between 3-D target surface, TARGE170, and a deformable surface, defined by this element.

Stability and Control Governing Equations

In this section, the governing equations for stability and control are given.

General Equations of Unsteady Motion

The general equations of unsteady motion of the airplane are written in the Body Axis System, Eqn. 4. The angular velocities are related to attitude angles, (ϕ, θ and ψ), through Eqn. 5. The rate of change of the CG position with respect to time, ($\dot{x}$, $\dot{y}$ and $\dot{z}$), measured with respect to Inertial Axis System, is given by Eqn. 6. Equations 4, 5, and 6 are taken directly from Ref. [10].

$$\begin{aligned}
&m(\dot{u}+qw-rv)+mg\sin\theta=X\\
&m(\dot{v}+ru-pw)-mg\cos\theta\sin\phi=Y\\
&m(\dot{w}+pv-qu)-mg\cos\theta\cos\phi=Z\\
&I_{XX}\dot{p}-I_{XZ}\dot{r}+(I_{ZZ}-I_{YY})qr-I_{XZ}pq=L\\
&I_{YY}\dot{q}+(I_{XX}-I_{ZZ})rq+I_{XZ}(p^2-r^2)=M\\
&-I_{XZ}\dot{p}+I_{ZZ}\dot{r}+(I_{YY}-I_{XX})pq+I_{XZ}qr=N
\end{aligned} \tag{4}$$

$$\begin{bmatrix}\dot{\phi}\\ \dot{\theta}\\ \dot{\psi}\end{bmatrix}=\begin{bmatrix}1 & sin\phi\ tan\theta & cos\phi\ tan\theta\\ 0 & cos\phi & -sin\phi\\ 0 & sin\phi\ sec\theta & cos\phi\ sec\theta\end{bmatrix}\begin{bmatrix}p\\ q\\ r\end{bmatrix} \tag{5}$$

$$\begin{bmatrix}\dot{x}\\ \dot{y}\\ \dot{z}\end{bmatrix}=\begin{bmatrix}cos\theta cos\psi & sin\phi sin\theta cos\psi-cos\phi sin\psi & cos\phi sin\theta cos\psi+sin\phi sin\psi\\ cos\theta sin\psi & sin\phi sin\theta sin\psi+cos\phi cos\psi & cos\phi sin\theta sin\psi-sin\phi cos\psi\\ -sin\theta & sin\phi cos\theta & cos\phi cos\theta\end{bmatrix}\begin{bmatrix}u\\ v\\ w\end{bmatrix} \tag{6}$$

Steady, Reference Flight Condition

The airplane is assumed to be in a state of steady flight, i.e., a state of motion such that Eqn. 7 is satisfied. This steady state of flight is termed the *Reference Flight Condition*, and may consist of any steady (such as steady rectilinear flight, steady side slip, level turns, and helical turns) or quasi-steady (for which the restrictions imposed by Eqn. 7 are only approximately satisfied, such as steady pull-up) maneuver.

$$\dot{u}=\dot{v}=\dot{w}=\dot{p}=\dot{q}=\dot{r}=0 \tag{7}$$

The equations of motion for a rigid airplane in the Body Axis System for the steady, reference flight condition are then obtained by substituting Eqn. 7 into Eqn. 4, as expressed in Eqn. 8. The subscript 1 denotes evaluation in the reference flight condition.

$$\begin{aligned}
&m(q_1w_1-r_1v_1)+mg\sin\theta_1=X_1\\
&m(r_1u_1-p_1w_1)-mg\cos\theta_1\sin\phi_1=Y_1\\
&m(p_1v_1-q_1u_1)-mg\cos\theta_1\cos\phi_1=Z_1\\
&\left(I_{ZZ_1}-I_{YY_1}\right)q_1r_1-I_{XZ_1}p_1q_1=L_1\\
&\left(I_{XX_1}-I_{ZZ_1}\right)r_1p_1+I_{XZ_1}(p_1^2-r_1^2)=M_1\\
&\left(I_{YY_1}-I_{XX_1}\right)p_1q_1+I_{XZ_1}q_1r_1=N_1
\end{aligned} \tag{8}$$

Linear Aerodynamic Forces and Moments

The linear aerodynamic theory requires that the components of aerodynamic force and couple be linear functions of the airplane's motion and the control surface settings. Also, motions of control surface settings which are symmetric with respect to the plane of symmetry of the airplane can give rise only to symmetric distributions of aerodynamic pressure, while antisymmetric motions and control surface settings produce only antisymmetric aerodynamic pressure distributions. The nonlinear aerodynamic terms, therefore, reduce to the linear forms given by Eqn. 9. The coefficients of the motion variables and control surface settings are all constants. The superscript A means aerodynamic components.

$$\begin{aligned}
X_1^A &= X_0^A + X_\alpha^A \alpha_1 + X_q^A q_1 + X_{\delta e}^A \delta e_1 \\
Y_1^A &= Y_\beta^A \beta_1 + Y_p^A p_1 + Y_r^A r_1 + Y_{\delta a}^A \delta a_1 + Y_{\delta r}^A \delta r_1 \\
Z_1^A &= Z_0^A + Z_\alpha^A \alpha_1 + Z_q^A q_1 + Z_{\delta e}^A \delta e_1 \\
L_1^A &= L_\beta^A \beta_1 + L_p^A p_1 + L_r^A r_1 + L_{\delta a}^A \delta a_1 + L_{\delta r}^A \delta r_1 \\
M_1^A &= M_0^A + M_\alpha^A \alpha_1 + M_q^A q_1 + M_{\delta e}^A \delta e_1 \\
N_{ZB_1}^A &= N_\beta^A \beta_1 + N_p^A p_1 + N_r^A r_1 + N_{\delta a}^A \delta a_1 + N_{\delta r}^A \delta r_1
\end{aligned} \tag{9}$$

where α is angle of attack, β is angle of side-slip; and δe, δa and δr are elevator, aileron and rudder deflections, respectively.

These coefficients constitute the aerodynamic derivatives of an airplane which are coefficients in a truncated Taylor series expansion about the flight condition wherein all trim parameters, (u_1, α_1, β_1, p_1, q_1, r_1, ϕ_1, γ_1, T_1, δe_1, δa_1, δr_1), are set to zero except u_1; where γ is flight-path angle and T is thrust amplitude. The aerodynamic derivatives are, therefore, distinct from the stability derivatives because the latter are the result of perturbations about the reference flight condition wherein all of the trim parameters may be different from zero. The parameter used to measure static stability is Static Margin, SM, given by Eqn. 10.

$$SM = -\frac{c_{m_\alpha}}{c_{L_\alpha}} \tag{10}$$

Unsteady Perturbation Flight Condition

The equations of motion are linearized for use in stability and control analysis. It is assumed that the motion of the airplane consists of small deviations from a steady, reference flight condition. The steady, reference flight condition here may be a steady cruise, steady climb, or steady descent. It is possible to use the term steady because the time period of interest for dynamic stability and control studies is sufficiently small that atmospheric properties and mass properties can be assumed constant. As a consequence, the angle of attack, the elevator angle, and the Mach number are constant, and the pitch rate and the angle of attack rate are zero on the reference path. All the variables in the equations of motion are replaced by a reference value plus a perturbation or disturbance as in Eqn. 11.

$$u = u_1 + \Delta u \ldots \text{etc} \tag{11}$$

For simplicity, the prefix Δ is removed in this section and keeping in mind that the reference value is given a subscript 1.

The longitudinal equations of motion are expressed in Eqn. 12. The stability derivatives $X_{\dot{u}}$…etc, are defined in Ref. [4].

$$\begin{aligned}
&(1 - X_{\dot{u}})\dot{u} - X_u^* u - X_{\dot{w}}\dot{w} - X_w w + \left(-X_q + w_1\right)\dot{\theta} + (g\, cos\theta_1)\theta = X_{\delta e}\delta e \\
&-Z_{\dot{u}}\dot{u} - Z_u^* u + (1 - Z_{\dot{w}})\dot{w} - Z_w w + \left(-Z_q - u_1\right)\dot{\theta} + (g\, sin\theta_1)\theta = Z_{\delta e}\delta e \\
&-M_{\dot{u}}\dot{u} - M_u^* u - M_{\dot{w}}\dot{w} - M_w w + \dot{q} - M_q\dot{\theta} = M_{\delta e}\delta e
\end{aligned} \tag{12}$$

Applying Laplace transformation on Eqn. 12 leads to the equations of motion in a matrix form, Eqn. 13, where $q = s\theta$

.

$$\begin{bmatrix} (1-X_{\dot{u}})s - X_u^* & -X_{\dot{w}}s - X_w & (-X_q + w_1)s + g\,cos\theta_1 \\ -Z_{\dot{u}}s - Z_u^* & (1-Z_{\dot{w}})s - Z_w & (-Z_q - u_1)s + g\,sin\theta_1 \\ -M_{\dot{u}}s - M_u^* & -M_{\dot{w}}s - M_w & s^2 - M_q s \end{bmatrix} \begin{bmatrix} u \\ w \\ \theta \end{bmatrix} = \begin{bmatrix} X_{\delta e} \\ Z_{\delta e} \\ M_{\delta e} \end{bmatrix} \delta e \qquad (13)$$

By the same manner, the lateral-directional equations of motion after taking Laplace transform are expressed in Eqn. 14, where $\phi = \frac{p}{s} + \frac{r}{s} tan\theta_1$ and $\psi = \frac{1}{cos\theta_1}\frac{r}{s}$.

.

$$\begin{bmatrix} s - Y_v & -\dfrac{w_1 s + g\,cos\theta_1}{V_1} & \dfrac{u_1 s - g\,sin\theta_1}{V_1\,s} \\ -L'_\beta & s(s - L'_p) & -L'_r \\ -N'_\beta & -N'_p s & s - N'_r \end{bmatrix} \begin{bmatrix} \beta \\ \dfrac{p}{s} \\ r \end{bmatrix} = \begin{bmatrix} Y_{\delta a}^* & Y_{\delta r}^* \\ L'_{\delta a} & L'_{\delta r} \\ N'_{\delta a} & N'_{\delta r} \end{bmatrix} \begin{bmatrix} \delta a \\ \delta r \end{bmatrix} \qquad (14)$$

Aerodynamic Derivatives of Rigid Airplane

In this section, the aerodynamic derivatives of rigid airplane will be calculated using ANSYS CFX. The results are then verified with those obtained from wind-tunnel tests given by Refs. [5, 6, 7 and 8].

The aerodynamic derivatives are separated into two classes; longitudinal, ($C_{L_\alpha}, C_{D_\alpha}, C_{m_\alpha}$, $C_{L_q}, C_{D_q}, C_{m_q}$), and lateral-directional, ($C_{Y_\beta}, C_{l_\beta}, C_{n_\beta}$, $C_{Y_p}, C_{l_p}, C_{n_p}$, $C_{Y_r}, C_{l_r}, C_{n_r}$). In addition, the control surfaces' derivatives may be calculated.

The α Derivatives

The control volume will be as in Fig. 1. To verify the results, ANSYS CFX results are compared with wind-tunnel results obtained for the model given by Ref. [8]. The results are plotted in Fig. 2.

The q Derivatives

The control volume will be as in Fig. 3. To verify the results, ANSYS CFX results are compared with wind-tunnel results obtained for the model given by Ref. [5].

The β Derivatives

The control volume will be again as in Fig. 1. To verify the results, ANSYS CFX results are compared with wind-tunnel results obtained for the model given by Ref. [8].

The p Derivatives

The control volume will be as in Fig. 4. To verify the results, ANSYS CFX results are compared with wind-tunnel results obtained for the model given by Ref. [7].

The r Derivatives

The control volume will be as in Fig. 5. To verify the results, ANSYS CFX results are compared with wind-tunnel results obtained for the model given by Ref. [5].

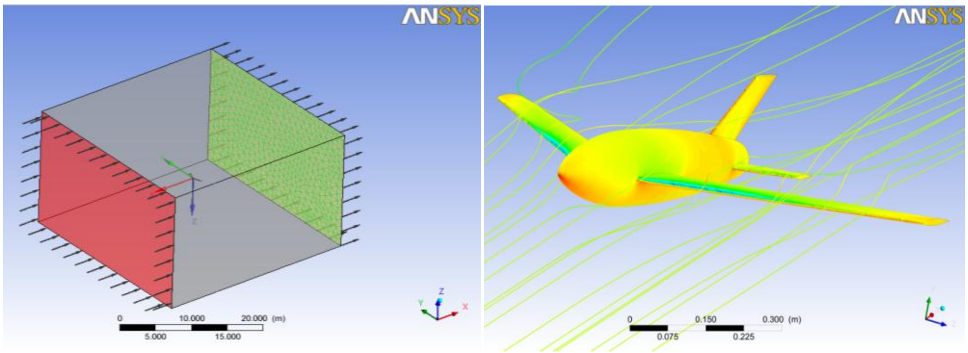

Fig. 1. The Control Volume and Verification Model for α and β Derivatives

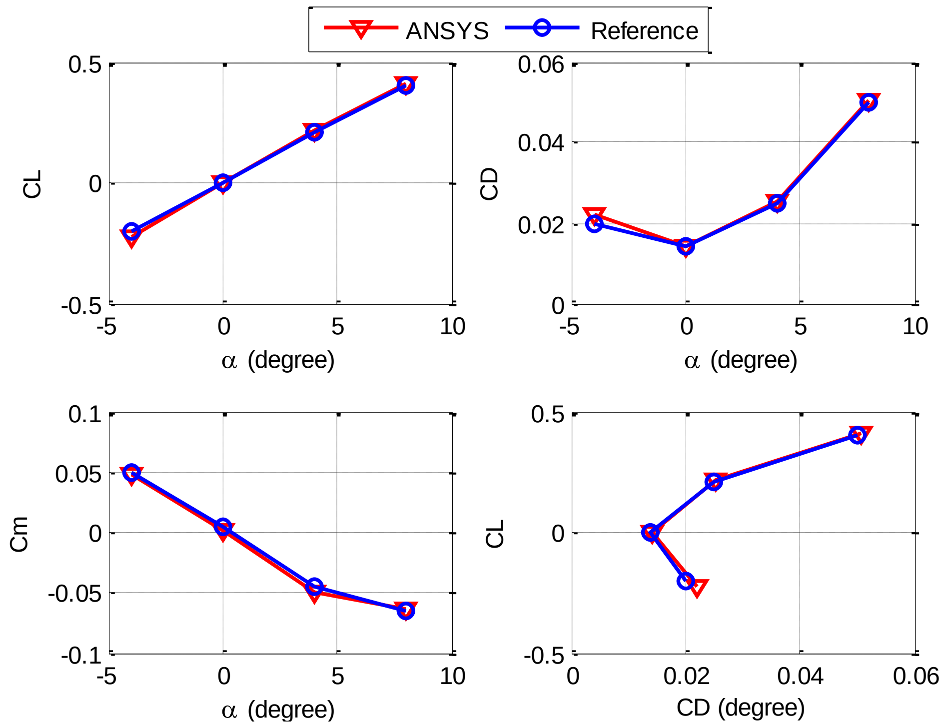

Fig. 2. The Results for α Derivatives

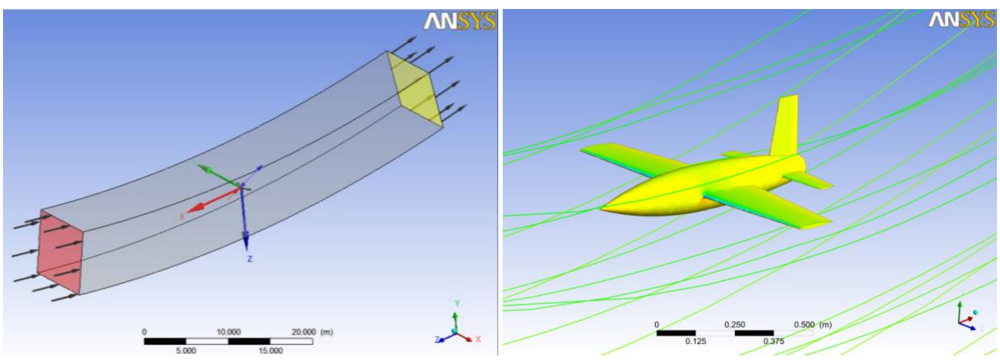

Fig. 3. The Control Volume and Verification Model for q Derivatives

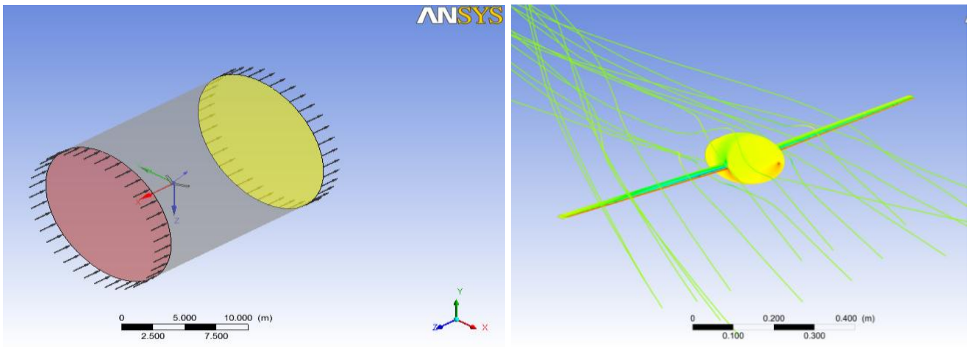

Fig. 4. The Control Volume and Verification Model for p Derivatives

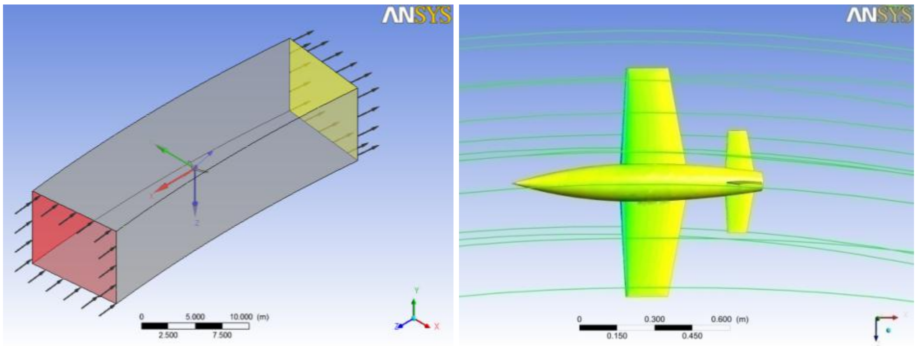

Fig. 5. The Control Volume and Verification Model for r Derivatives

Aerodynamic Derivatives of Flexible Airplane

In this section, the aerodynamic derivatives of flexible airplane will be calculated as functions in the dynamic pressure, q_∞. The analysis is done by coupling the aerodynamics with structure through a two-way fluid-structure interaction. ANSYS Multi-Field MFX is used as the calculation tool.

The Flexible Model Geometry

The flexible model which is used has the geometric characteristics given by Table 1 and shown in Fig. 6.

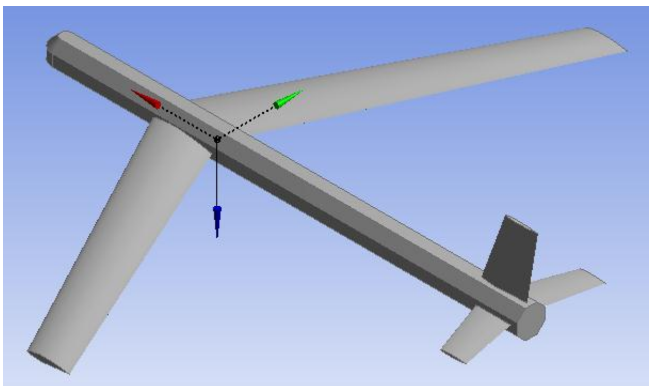

Fig. 6. The Flexible Model Aerodynamic Geometry

Table 1. The Flexible Model Geometric Characteristics

Parameter	Value
Wing	
Aspect Ratio	10.86
Taper Ratio	0.7
Span	30.48 (m)
Mean Aerodynamic Chord	2.8358 (m)
Sweep Back Angle at Leading Edge	30 (deg.)
Root Chord	3.302 (m)
Wing Area	85.548 (m2)
Washout Angle	-2.88 (deg.)
Wash-Out Distribution	Linear
Root Chord Incidence Angle to FRL	+1 (deg.)
Dihedral Angle	0 (deg.)
Airfoil	NACA 65-213
X Distance from Wing Apex to Fuselage Nose	5.842 (m)
Horizontal Tail	
Taper Ratio	0.7
Span	7.62 (m)
Sweep Back Angle at Leading Edge	20 (deg.)
Root Chord	2.032 (m)
Washout Angle	0 (deg.)
Root Chord Incidence Angle to FRL	-1 (deg.)
Airfoil	NACA 65A-008
X Distance from Wing Apex to Fuselage Nose	23.622 (m)
Vertical Tail	
Taper Ratio	0.7
Semi-Span	3.81 (m)
Sweep Back Angle at Leading Edge	20 (deg.)
Root Chord	2.54 (m)
Airfoil	NACA 65A-008
X Distance from Wing Apex to Fuselage Nose	23.368 (m)
Z Distance from Root Chord to FRL	0.508 (m)
Fuselage	
Cross Section	Regular Octagon
Cross Section Span (Octagon Shortest Diagonal)	1.524 (m)
Straight-part Fuselage Length	25.4 (m)
Nose Length	0.762 (m)
Nose Shape	Revolved Semi-Octagon

The model spars and ribs are made from Polyethylene material while all the airplane skin is made from Aluminum Alloy. The model structure is shown in Fig. 7 and has the mass model given by Table 2.

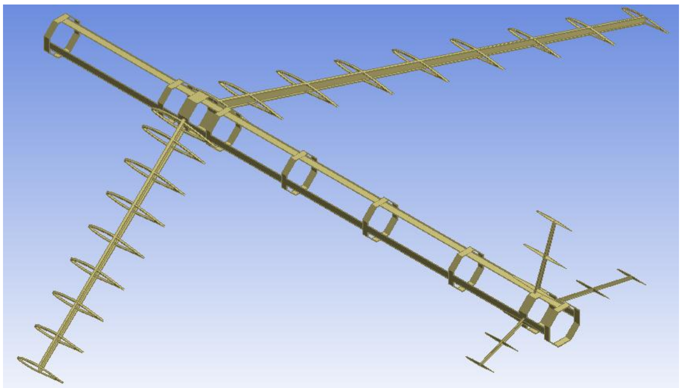

a)

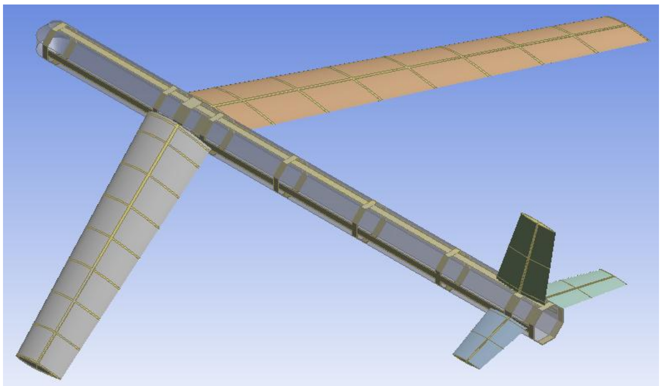

b)

Fig. 7. The Flexible Model Structure Geometry, a) Without Skin, b) With Skin

Table 2. The Flexible Model Mass Model

Parameter	Value
m (kg)	2629.4
I_X (kg.m^2)	109,479
I_Y (kg.m^2)	109,044
I_Z (kg.m^2)	216,806
I_{XZ} (kg.m^2)	2857
X_{CG} (m)	5.715
Y_{CG} (m)	0
Z_{CG} (m)	0

The Flexible Model Aerodynamic Derivatives

In this and the following sections, the aerodynamic derivatives for the flexible airplane model will be calculated for four combinations of dynamic pressure as in Table 3. Also the aerodynamic derivatives for the rigid airplane will be calculated and compared with the flexible one. The α derivatives are given as ratio, e.g., $\left(C_{L_\alpha}\right)_{\text{Flexible}}/\left(C_{L_\alpha}\right)_{\text{Rigid}}$, and plotted versus dynamic pressure. The results are shown in Figs. 8 through 12.

Table 3. Dynamic Pressure (Flight Condition) Combinations

Flight Cond. No.	Altitude (km)	Velocity (m/s)	Dynamic Pressure (N/m^2)
Flexible 1	10	50	516.9
Flexible 2	Sea Level	50	1531.3
Flexible 3	10	100	2067.6
Flexible 4	Sea Level	100	6125

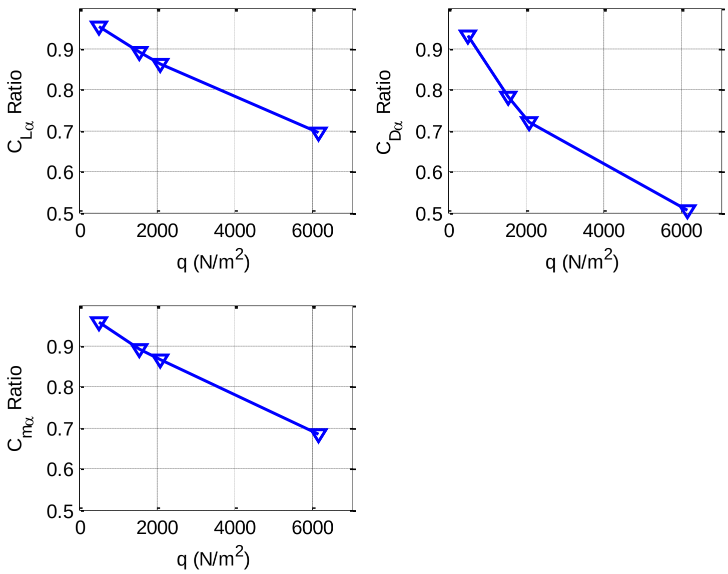

Fig. 8. The α Derivatives Ratio vs. Dynamic Pressure

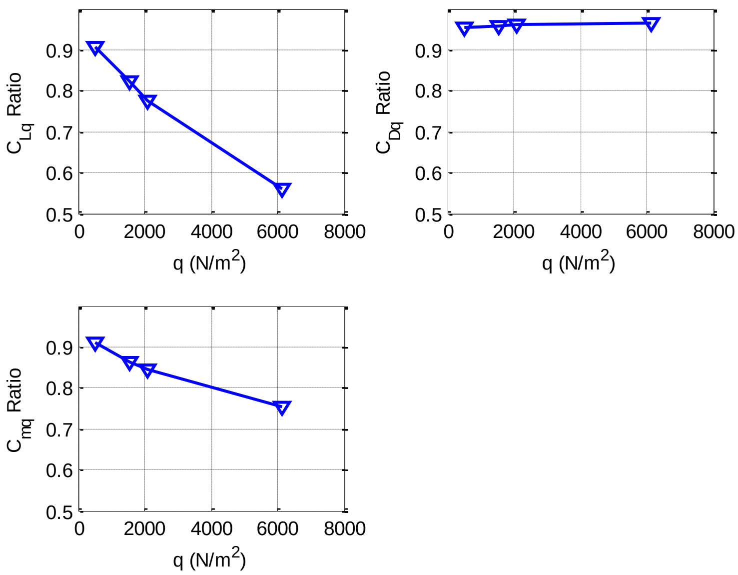

Fig. 9. The q Derivatives Ratio vs. Dynamic Pressure

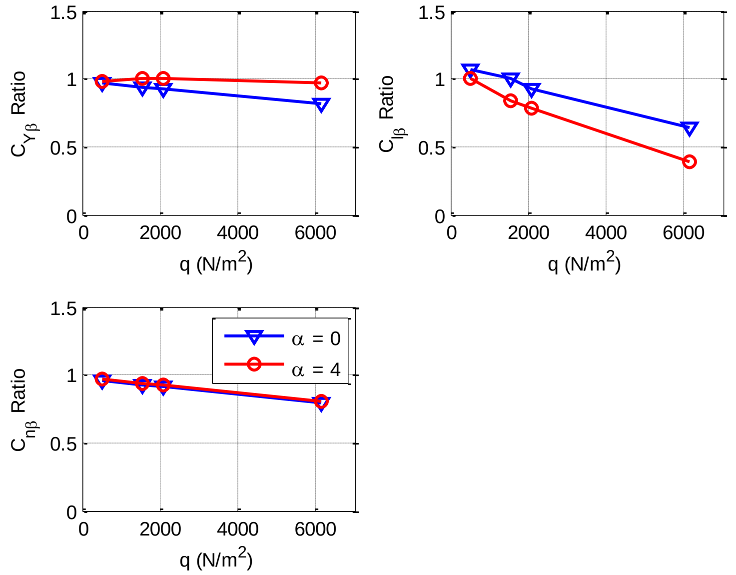

Fig. 10. The β Derivatives Ratio vs. Dynamic Pressure

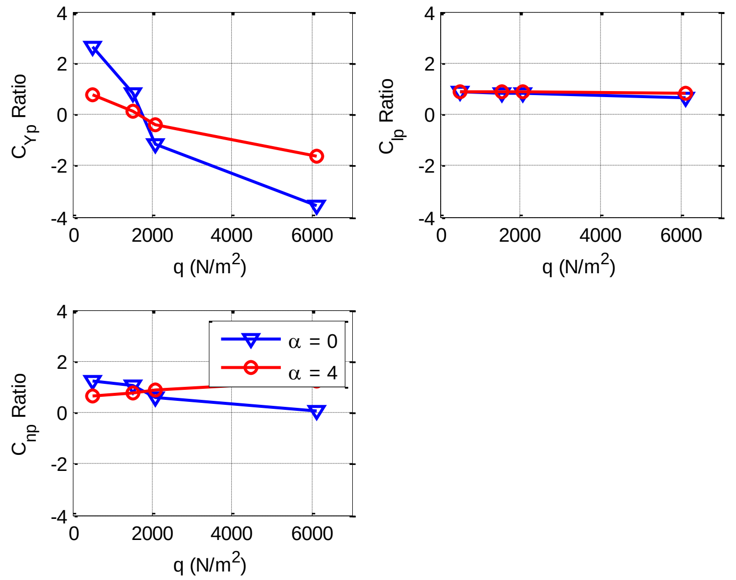

Fig. 11. The p Derivatives Ratio vs. Dynamic Pressure

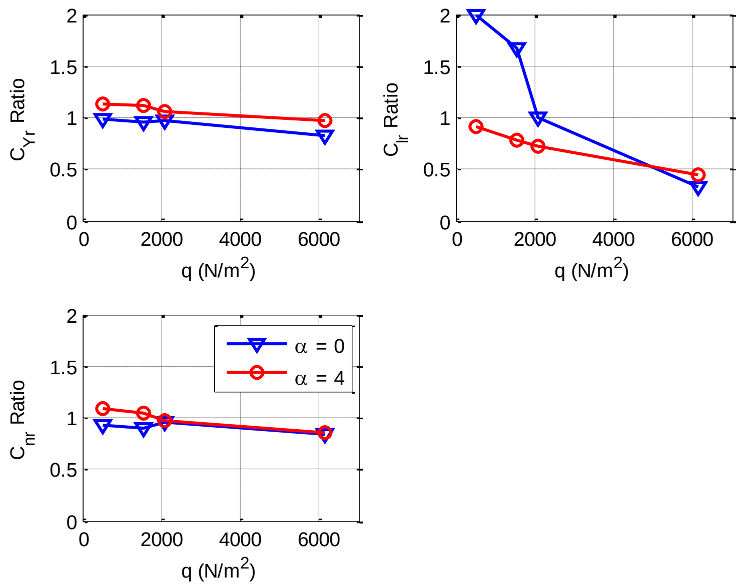

Fig. 12. The r Derivatives Ratio vs. Dynamic Pressure

Stability and Control of the Flexible Model

In this section, stability and control of the flexible model is examined.

Static Stability

The static margin ratio is plotted in Fig. 13 showing a small decrease in static stability with dynamic pressure variation.

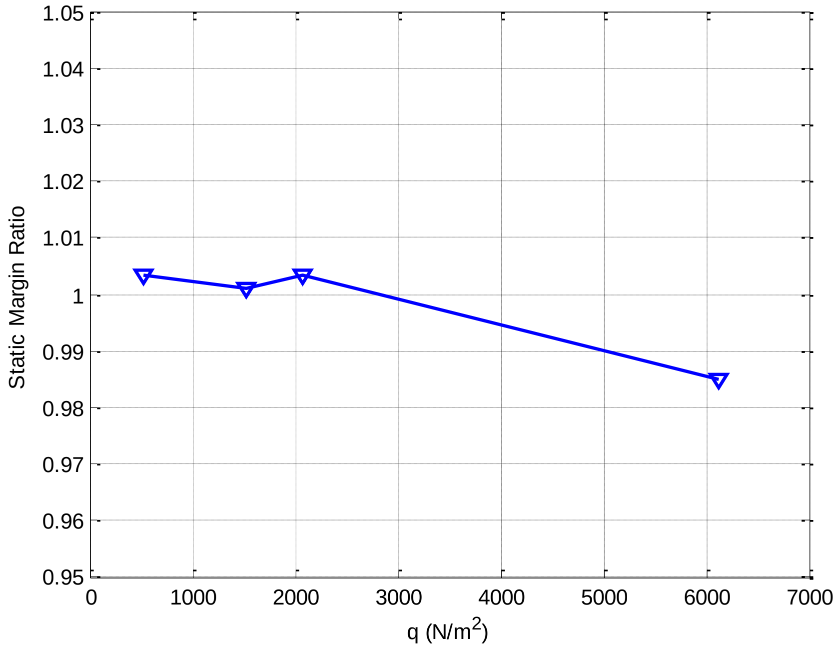

Fig. 13. Static Margin Ratio vs. Dynamic Pressure

Dynamic Stability

Longitudinal and lateral-directional modes are calculated and given in Tables 4 and 5, respectively.

Table 4. Longitudinal Characteristic Roots Variation with Dynamic Pressure

Flight Cond. No.	Phugoid	Short Period
Rigid	$-0.052 \pm 0.0639i$	$-10.6 \pm 7.93i$
Flexible 1 ($q_\infty = 516.9$)	$-0.0119 \pm 0.222i$	$-1.68 \pm 2.26i$
Flexible 2 ($q_\infty = 1531.2$)	$-0.0267 \pm 0.172i$	$-4.67 \pm 3.75i$
Flexible 3 ($q_\infty = 2067.6$)	$-0.0175 \pm 0.111i$	$-3.07 \pm 4.28i$
Flexible 4 ($q_\infty = 6125$)	$-0.0515 \pm 0.0737i$	$-7.70 \pm 6.56i$

Table 5. Lateral-Directional Characteristic Roots Variation with Dynamic Pressure

Flight Cond. No.	Spiral	Dutch Roll	Rolling
Rigid	-0.0047	$-2.03 \pm 3.79i$	-12.6
Flexible 1 ($q_\infty = 516.9$)	-0.0185	$-0.287 \pm 1.11i$	-1.76
Flexible 2 ($q_\infty = 1531.2$)	-0.00616	$-0.92 \pm 1.83i$	-5.19
Flexible 3 ($q_\infty = 2067.6$)	-0.00520	$-0.619 \pm 2.13i$	-3.53
Flexible 4 ($q_\infty = 6125$)	-0.00713	$-1.69 \pm 3.35i$	-7.92

Design of Automatic Flight Control Systems

An example automatic flight control system, pitch-attitude hold, is designed for the flexible airplane at the different values of dynamic pressure. The block diagram suggested for this autopilot mode is given in Fig. 14 and added to it a limiter for the reference input in order to prevent the angle of attack from getting into stall region. The elevator servo break frequency is assumed to be $a = 10\,rad/sec$, while the pitch attitude gyro gain is assumed to be $K_{gyro} = 1$. The transfer function $\frac{\theta}{\delta_e}$ is in the form $\frac{A_\theta S^2+B_\theta S+C_\theta}{S^4+AS^3+BS^2+CS+D}$. The denominator coefficients can be calculated from the transfer function characteristic roots represented earlier in Table 4, while the numerator coefficients are written in Table 6.

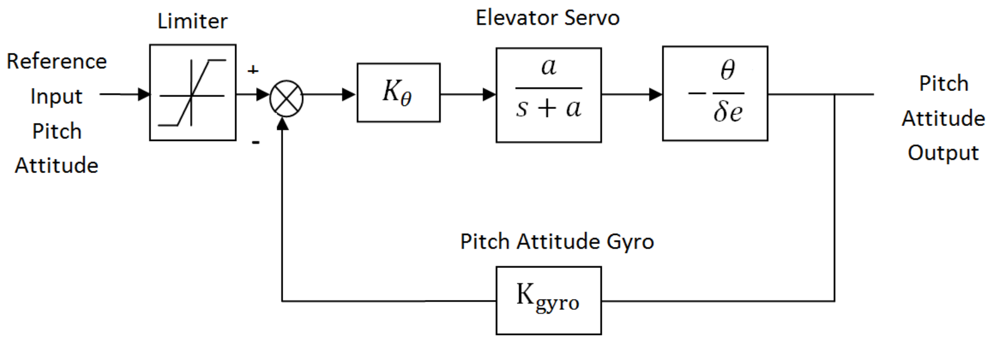

Fig. 14. Block Diagram for Pitch-Attitude-Hold AFCS

Table 6. Numerator Coefficients for $\frac{\theta}{\delta_e}$ Transfer Function at Different Flight Conditions

Coefficient	Rigid	Flexible 1	Flexible 2	Flexible 3	Flexible 4
A_θ	-21	-1.772	-5.251	-7.09	-21
B_θ	-196.4	-2.719	-21.99	-19.34	-137.8
C_θ	-21	-1.772	-5.251	-7.09	-21

The design requirements for this pitch-attitude hold AFCS are chosen for the Phugoid poles to be critically damped. The values of K_θ that will satisfy design requirements (Gain Scheduling) are given in Table 7. In addition, the steady state error for unit step input at these values of K_θ is given.

Table 7. K_θ to Satisfy Design Requirements at Different Flight Conditions

Flight Cond. No.	K_θ	$e_{ss}\%$
Rigid	0.28	16
Flexible 1 ($q_\infty = 516.9$)	2.28	40
Flexible 2 ($q_\infty = 1531.2$)	0.814	40
Flexible 3 ($q_\infty = 2067.6$)	0.452	43
Flexible 4 ($q_\infty = 6125$)	0.245	16

The flexibility effect on system dynamics for the transfer function $\frac{\theta}{\delta_e}$ can be shown as in Fig. 15. Also the dynamic response for the pitch attitude hold AFCS system (after using gain scheduling) can be shown as in Fig. 16.

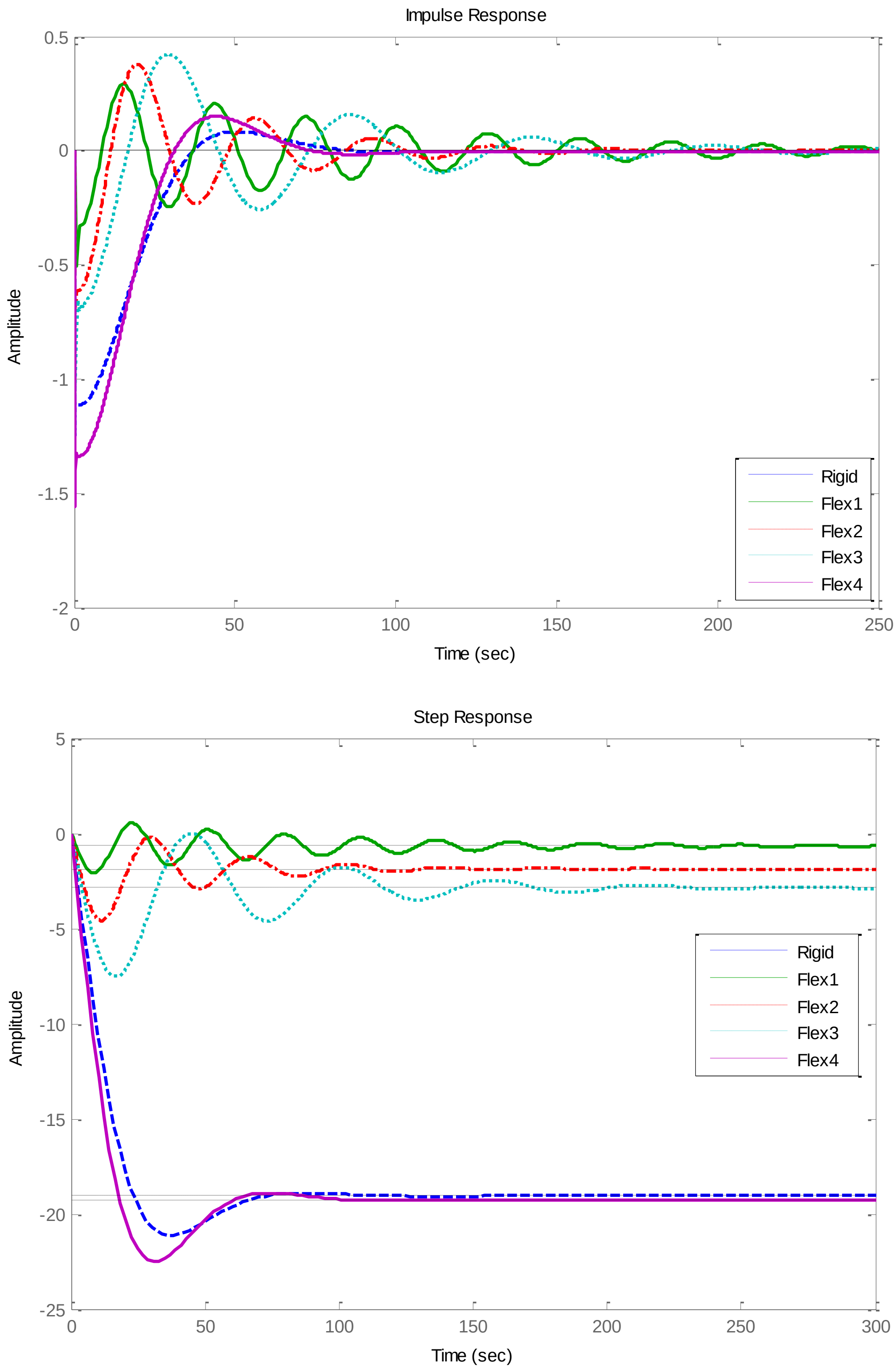

Fig. 15. Impulse and Step Responses for $\frac{\theta}{\delta_e}$ showing the flexibility effect

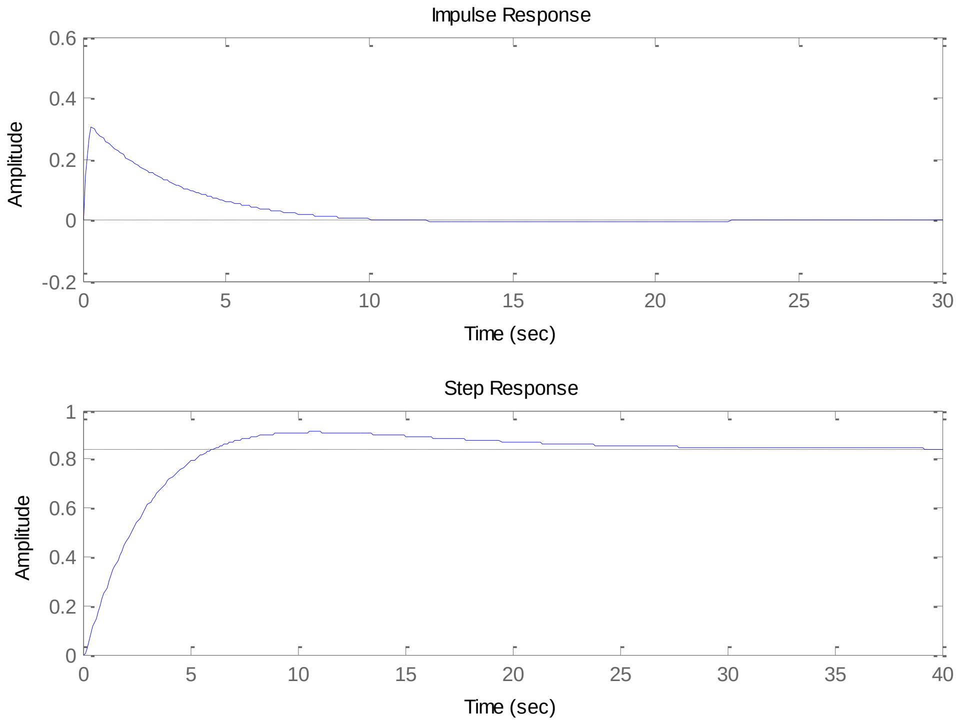

Fig. 16. Impulse and Step Responses for Pitch Attitude Hold AFCS (after using Gain Scheduling)

Flight Simulation

The equations of motion are solved to get the motion variables with time for a prescribed path or prescribed control settings. The solution is done by using fourth order Runge-Kutta numerical integration. For a symmetric motion, the equations of motion in the Body Axis System are given by Eqns. 15, 16 and 17. In addition, three other equations are given by Eqn. 18.

$$\begin{aligned} \dot{u} &= \frac{X}{m} - g \sin\theta - qw \\ \dot{w} &= \frac{Z}{m} + g\cos\theta + qu \\ \dot{q} &= \frac{M}{I_{YY}} \end{aligned} \tag{15}$$

$$\dot{\theta} = q \tag{16}$$

$$\begin{aligned} \dot{x} &= u\cos\theta + w\sin\theta \\ \dot{z} &= -u\sin\theta + w\cos\theta \end{aligned} \tag{17}$$

$$\begin{aligned} \dot{V} &= \frac{(u\,\dot{u} + w\,\dot{w})}{V} \\ \dot{\alpha} &= \frac{u\dot{w} - w\dot{u}}{u^2 + w^2} \\ \dot{\gamma} &= \dot{\theta} - \dot{\alpha} \end{aligned} \tag{18}$$

The results for a pull-up maneuver for Rigid and Flexible 1 flight conditions are shown in Fig. 17.

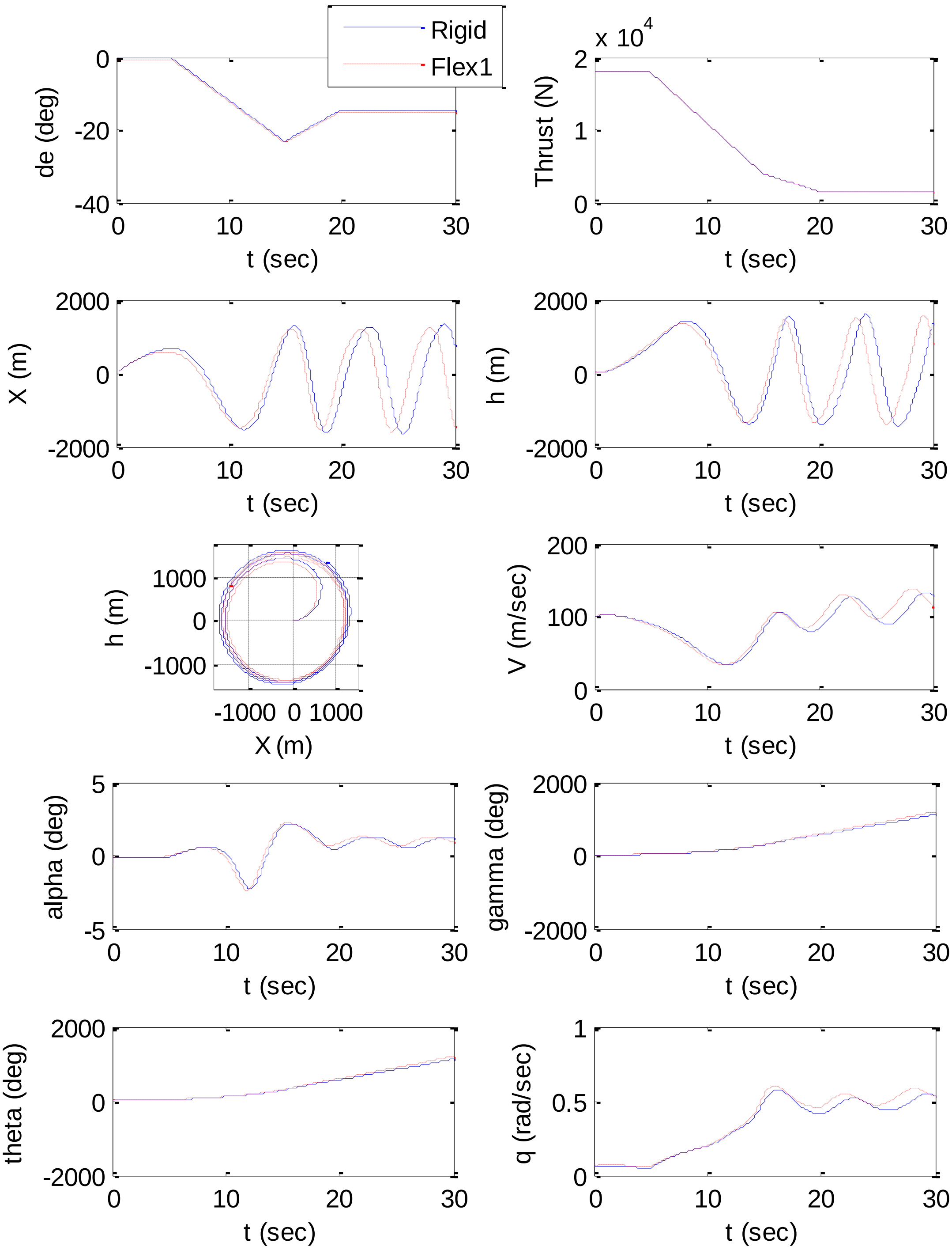

Fig. 17. Pull-up Maneuver Simulation using Runge-Kutta Numerical Integration

Conclusions

- For a flexible airplane, the aerodynamic derivatives are no longer only functions in normal parameters, such as angle of attack; instead they become functions in additional parameter, the dynamic pressure.
- For the same configuration, a flexible airplane has less static and dynamic stability than a rigid one. The percentage change depends on how much the airplane is flexible.
- The effect of flexibility on dynamic stability can be reduced by using gain scheduling when designing the airplane's automatic flight control systems.
- To get a certain aerodynamic, stability and control characteristics for an airplane in the design point flight condition, the Jig Shape has to be calculated.
- The jig shape is computed by solving the trim problem for the design point flight condition with the airplane treated as a rigid body having the design shape. The resulting aerodynamic and propulsion system loads are then applied on the airplane leading to deformation (displacement). The displacements computed are subtracted from the design shape coordinates. These operations establish the jig coordinates.

References

[1] Patil, M.J. and Hodges, D.H., "Flight Dynamics of Highly Flexible Flying Wings", *Journal of Aircraft*, November, 2006, Vol. 43, No. 6.

[2] Chang, C.S., Hodges, D.H. and Patil, M.J., "Flight Dynamics of Highly Flexible Aircraft", *Journal of Aircraft*, 2008, Vol. 45, No. 2.

[3] Boeing D6-41064-1 and NASA CR-114712, "A Method for Predicting the Stability Characteristics of an Elastic Airplane: Volume I FLEXSTAB Theoretical Description", 1974.

[4] NASA CR-2144, "Aircraft Handling Qualities Data", 1972.

[5] Fletcher, H.S., NASA TN D-6531, "Comparison of Several Methods for Estimating Low-Speed Stability Derivatives for Two Airplane Configurations", 1971.

[6] Letko, W. and Riley D.R., NACA TN-2175, "Effect of an Unswept Wing on the Contribution of Unswept-Tail Configuration to the Low-Speed Static- and Rolling-Stability Derivatives of a Mid-wing Airplane Model", 1950.

[7] Wiggins, J.W., NACA TN-4185, "Wind Tunnel Investigation of Effect of Sweep on Rolling Derivatives at Angles of Attack up to 13° and at High Subsonic Mach Numbers, Including a Semi-empirical Method of Estimating the Rolling Derivatives", 1958.

[8] Wolhart, W.D. and Thomas D.F., NACA TN-4397, "Static Longitudinal and Lateral Stability Characteristics at Low-Speed of 60 Sweptback Mid-wing Models having Wings with an Aspect ratio 2, 4, or 6", 1958.

[9] ANSYS Inc., "ANSYS Workbench 12 User's Manual", 2009.

[10] Etkin, B. and Reid, L.D., *Dynamics of Flight Stability and control*, 3rd ed., Wiley, New York, 1996.

[11] Stevens, B.L. and Lewis, F.L., *Aircraft Control and Simulation*, 3rd ed., Wiley, New York, 1992.